J Mater Sci (2021) 56:11377–11385

Computation & theory

Theoretical study of the strain influence on lead-free bismuth-based halide perovskites

Xiaoyu Wang[1], Gang Bi[2], Nasir Ali[1], Yansong Chen[1], and Huizhen Wu[1,*]

[1] Zhejiang Province Key Laboratory of Quantum Technology and Devices, Department of Physics, and State Key Laboratory of Silicon Materials, Zhejiang University, Hangzhou 310027, Zhejiang, People's Republic of China

[2] School of Information and Electrical Engineering, Zhejiang University City College, Hangzhou 310015, Zhejiang, People's Republic of China

Received: 8 December 2020
Accepted: 17 March 2021
Published online: 29 March 2021

ABSTRACT

The existence of bio-accumulative lead hinders the commercialization of optoelectronic applications of Pb-based halide perovskites (PVKs). Therefore, researchers are seeking for comparative lead-free PVKs. Owing to the identical electronic configuration with Pb, Bi-based PVKs are proved to be one of the most promising candidates. Because strain is widely existed altering materials' characteristics, it is crucial to study the influences of strain on the Bi-based PVKs. Our theoretical work investigates the strain influences on two kinds of Bi-based PVKs, i.e., $Cs_3Bi_2Br_9$, and $Cs_2BiAgBr_6$. It is observed that both the tensile and compressive strains effectively change the crystal structures and the bandgaps, i.e., enlargement under tensile strain while shrinkage under compressive strain. Simultanously, the absorption spectra of these PVKs are also discussed. The strain study of Bi-based PVKs will offer guidance to the further development of lead-free PVKs.

Introduction

Halide perovskites (PVKs) are emerging as promising next-generation optoelectronic materials due to their extraordinary optoelectronic properties [1]. However, the presence of toxic-Pb vagues their commercialization and scalability. To address this issue, numerous lead-free PVKs have been introduced [2]. Unlike the conventional Pb-based PVKs, lead-free PVKs are eco-friendly and possess enormous potentials for large-scale optoelectronic applications. Among them, homovalent Sn^{2+} has successfully substituted the toxic Pb^{2+} and enabled the PVK to retain its 3D ABX_3 structure, where, A = (methylammonium or MA^+, formamidinium or FA^+, Cs^+), B = (Pb^{2+}, Sn^{2+}), and X = (Cl^-, Br^- or I^-). Preliminary studies on Sn-based lead-free PVKs showed some promises in optoelectronic devices (e.g., in photovoltaics) [3]. Unfortunately, due to their

Handling Editor: Yaroslava Yingling.

Address correspondence to E-mail: hzwu@zju.edu.cn

https://doi.org/10.1007/s10853-021-06025-7

rapid oxidation from Sn^{2+} to Sn^{4+} in ambient conditions, they cannot retain their ABX_3 structure and convert into other phases, which are unfavorable for optoelectronic applications.

To cope with this issue, Bi^{3+} with a similar electronicity to Pb^{2+} (i.e., filled 6 s orbitals and almost empty p-orbitals) and better environmental stability has been introduced into PVKs [4]. Bi-based PVKs have been synthesized in the forms of single crystals, films, and nanocrystals, which are employed in solar cells and photodetectors, etc. [4]. Since Bi^{3+} possesses different valency than that of Pb^{2+}, Bi^{3+}-based heterovalent-substituted PVKs share a chemical formula $A_3Bi_2X_9$ other than ABX_3 and exhibit different lattice structures with lower dimensionalities [4]. To balance the valences and maintain the cubic lattice structures (which often exhibit better electronic transportation), an additional monovalent metal cation (e.g., Ag^+ and Na^+) is introduced into the B-site of PVK framework. Consequently, PVKs with a chemical formula $A_2B'B''X_6$ ($B' = Bi^{3+}$ or Sb^{3+}, $B'' = Ag^+$ or Na^+) are constituted. Because of two different kinds of metal cations occupying the B-site, these PVKs are named as double perovskites (DPVKs).[5] Among various DPVKs, combinations like Bi^{3+}/Ag^+, In^{3+}/Ag^+, and Sb^{3+}/Ag^+ have been reported as stable lead-free PVKs [5]. On account of the rich combinations of DPVKs, a giant prospect is expected and the theoretical prediction of the novel DPVKs plays an important role in the development of lead-free PVKs [5].

In practical situations, due to some external factors, i.e., bend or stretch, and fabrication procedures, e.g., during crystallization, strains are widely generated in functional materials, influencing the material properties [6]. Materials like oxides as well as two-dimensional materials are extensively investigated under external strains, which effectively modify their properties [7, 8]. However, halide PVKs are scarcely studied under strains. For instance, strained epitaxial growth of $FAPbI_3$ was studied and strain engineering was applied to enhance the performance of photodetectors [9]. Similarly, the influence of strain on the optical and electrical properties of $CH_3NH_3PbI_3$ and 2D PVKs are studied [10–12], and 2D PVK-based strain sensor was successfully fabricated [13]. As far as the study of lead-free PVKs under strain is concerned, $Cs_2InAgCl_6$ is theoretically investigated and bandgap variation was observed [14]. Therefore, we believe that strains will also influence Bi-based PVKs. To the best of our knowledge, there are few studies available in the literature about the effects of strain on Bi-based PVKs [15]. Thus, it is vital to explore the evolution in their structural and optoelectronic characteristics under strains, which is of great significance for a further understanding and their optoelectronic applications.

In this work, we investigate theoretically the influences of strain on two typical kinds of Bi-based PVKs, i.e., $Cs_3Bi_2Br_9$ and $Cs_2BiAgBr_6$, by first-principle calculations. We choose $Cs_3Bi_2Br_9$ and $Cs_2BiAgBr_6$ because, they do not contain any organic moieties, are environmentally stable, and show promises for various optoelectronic applications [4]. It is observed that both the tensile and compressive strains effectively change the widths of the bandgaps, i.e., enlargement under tensile strain while shrinkage under compressive strain. With a combination of the density of states and bandgaps, the absorption spectra of two Bi-based PVKs are also discussed.

Computational details

Density functional theory (DFT) based on the Perdew–Burke–Ernzerhof (PBE) generalized gradient approximation (GGA) [16] with interactions between ion cores and valence electrons described by the projector augmented wave (PAW) method [17] as implemented in the VASP software package [18] was employed in the present work. For $Cs_2BiAgBr_6$ and $Cs_3Bi_2Br_9$, Γ-centered $5 \times 5 \times 5$ and $5 \times 5 \times 3$ k-meshes were used, respectively. The cutoff energy is 520 eV and structural optimizations were stopped when all the total forces on each atom were below 0.01 eV/Å. The convergence accuracy is 1×10^{-5} eV. After fully relaxations, the lattice parameters were adjusted to simulate the hydrostatic strains from -10% to 10% with a 5% interval, and the atoms are next fully relaxed. The crystal structures were visualized using VESTA [19].

Results and discussions

Based on previous studies, stable $Cs_3Bi_2Br_9$ has a trigonal $P\bar{3}m1$ symmetry, where 2D layered corner-sharing $[BiBr_6]$ octahedra are surrounded by Cs^+.[20] This kind of PVKs is called vacancy-ordered PVKs and compared with conventional PVKs, only two-

thirds of the octahedral positions are fully occupied. The reported experimental results indicate that $Cs_3Bi_2Br_9$ has a direct and allowed band-gap transition with the energy of about 2.61 eV, and especially in colloidal nanocrystal (NC) form, $Cs_3Bi_2Br_9$ has a high photoluminescence quantum yield (PLQY), showing promises in illumination applications [21]. In our calculation, first of all, a primitive cell of $Cs_3Bi_2Br_9$ is modeled, fully optimized, and employed as the unstrained $Cs_3Bi_2Br_9$ structure. In the electronic configuration analyses, as Fig. 1 exhibited, a hybrid of Bi s-orbitals and Br p-orbitals mainly contributes to the valence band maximum (VBM) and a hybrid of Bi p-orbitals and Br p-orbitals contributes to the conduction band minimum (CBM), which are obtained from the density of states (DOS) of the unstrained $Cs_3Bi_2Br_9$. In the band structure, both the VBM and CBM are located at the Γ point. It is worth noting that in the k-path from K to Γ in CBM, the energy varies slowly and keeps almost the same near point Γ, which may result in simultaneously direct and indirect transitions. This predicted phenomenon was observed in $Cs_3Bi_2Br_9$ NCs in the previous report [22]. In addition, the bandgap is theoretically estimated as 2.60 eV, close to the experiment result [21].

To stimulate the strains applied on $Cs_3Bi_2Br_9$, including tensile and compressive ones, the lattice parameters are adjusted accordingly. The applied strains are estimated by $\varepsilon = \frac{a-a_0}{a_0}$, where a is the adjusted lattice parameter and a_0 is the original lattice parameter. In order to distinguish the strain influences, 5% strain interval has been chosen and strain-free, 5% and 10% of compressive as well as tensile strains are considered. The tensile and compressive strains are differentiated by their positive and negative values, respectively. The crystal structures as well as electronic properties are characterized after full optimizations. Firstly, as exhibited in Fig. 2, the bandgap of $Cs_3Bi_2Br_9$ varies under strains, e.g., the bandgap increases under tensile strains and decreases when the compressive strains are applied. Unlike Pb-based PVK $(CH_3NH_3)PbI_3$, of which the direct bandgap is kept under strains [10], the band edge transition changes from direct to indirect under compressive strains. The valance band edge from point K to Γ raises, surpassing the energy at point Γ, which is the VBM of unstrained $Cs_3Bi_2Br_9$. Although the conduction bands get lower under compressive strains, CBM is still at point Γ, resulting in an indirect band edge transition. On the other hand, the tensile strain will make both the conduction and valence bands more flat, without changing the direct band edge transition.

On account of a hybrid of Bi and Br orbitals mainly contributes electronic states in VBM and CBM, we consider that the $[BiBr_6]$ octahedra will play a key role in electronic characteristics under strain. Unlike conventional PVK $CsPbBr_3$, we find the $[BiBr_6]$ octahedra are not regular and three shorter and longer bonds are divided into two types; named as Bond1 and Bond2 (Fig. 3a), exhibiting different covalent interaction strengths [23]. The crystal structures under different strains are subsequently studied and the variations of bond lengths of Bi–Br are exhibited in Fig. 3b. Interestingly, it is observed that the Bond1 length decreases under both tensile and compressive strains, but the Bond2 length increases monotonously from 10%-compressive to 10%-tensile strains. We assume that because of different covalent interaction strengths that exist in strain-free $Cs_3Bi_2Br_9$, the tensile strain has enlarged the differences between two Bi–Br bond types, resulting in the formation of $[BiBr_3]$

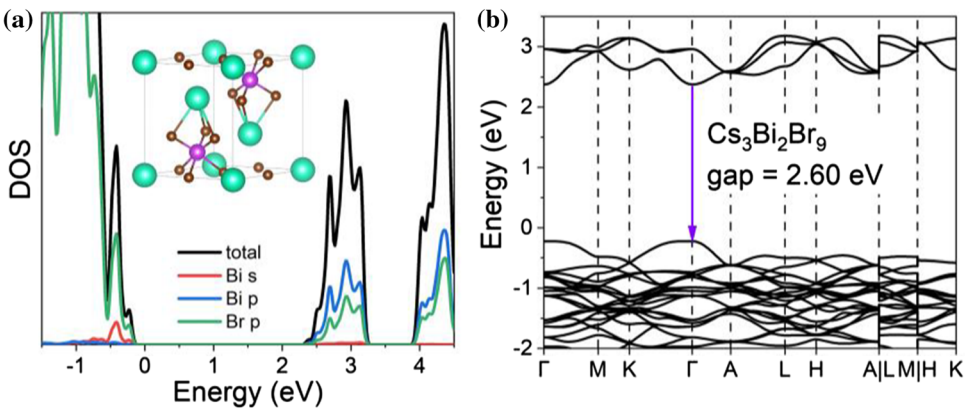

Figure 1 **a** The DOS diagram of the unstrained $Cs_3Bi_2Br_9$. Inset: the diagram of the unstrained $Cs_3Bi_2Br_9$ structure. **b** The diagram of the band structure of unstrained $Cs_3Bi_2Br_9$.

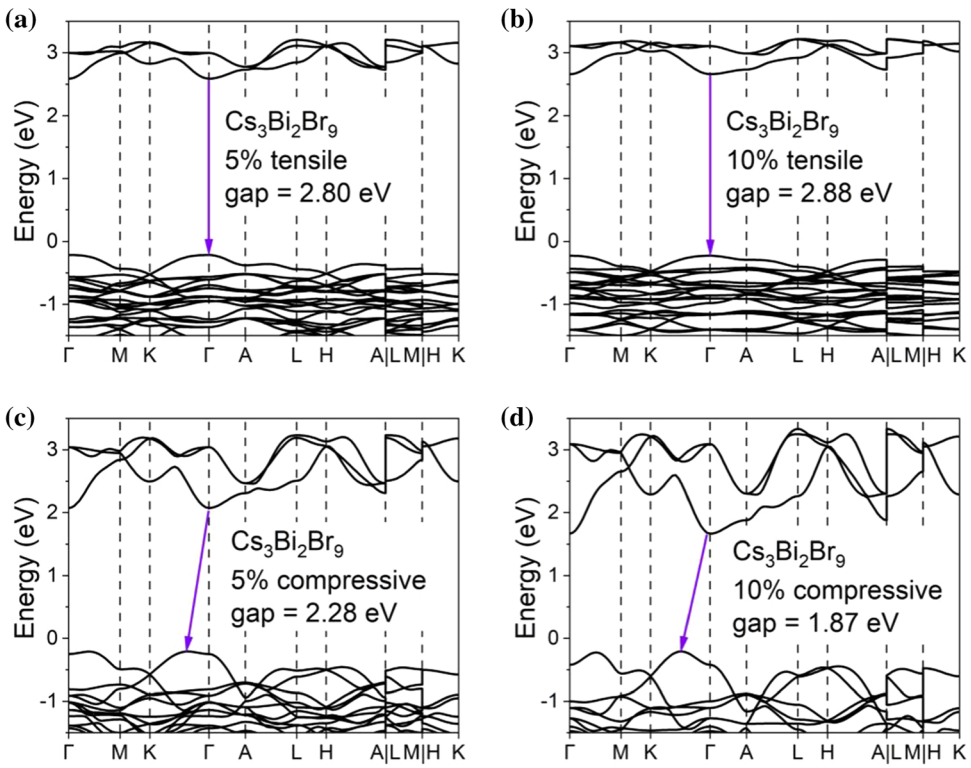

Figure 2 The energy band structures of $Cs_3Bi_2Br_9$: under **a** 5% tensile, **b** 10% tensile, **b** 5% compressive and **d** 10% compressive strains, respectively.

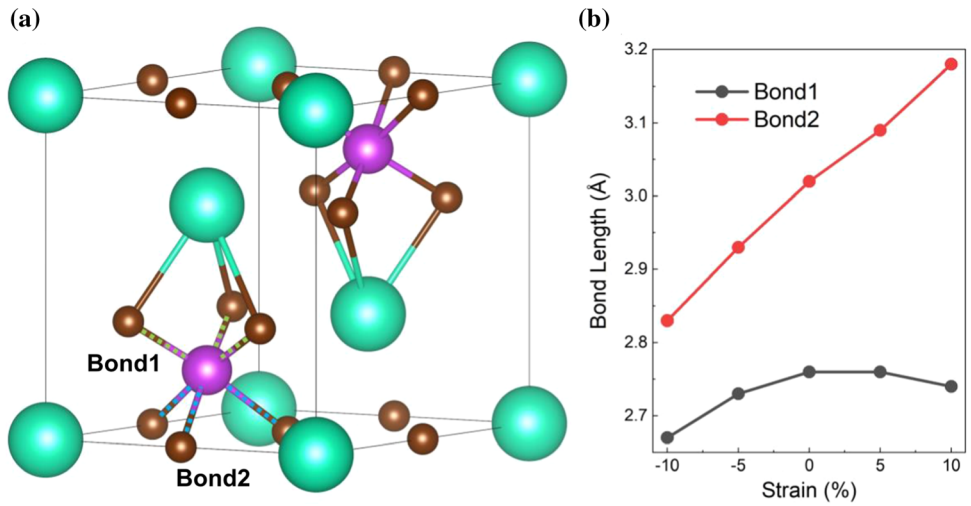

Figure 3 **a** The schematic diagram of Bi–Br bonds in $Cs_3Bi_2Br_9$, where the shorter and longer Bi–Br bonds are marked with green and blue dash lines and named as Bond1 and Bond2, respectively. **b** The Bi–Br bond lengths in $Cs_3Bi_2Br_9$ under strains.

tetrahedra same as zero-dimensional (0D) copper- or zinc-based PVKs [24, 25]. These 0D PVKs often have higher bandgaps and flattened band edges, similar to $Cs_3Bi_2Br_9$ under tensile strain. Under compressive strain, the $Cs_3Bi_2Br_9$ structure mentioned above is kept with shrinkages of the bond lengths. Smaller bond lengths will enhance the atomic interactions, leading toward a variation in electronic bands. We suppose these stronger interactions lead the shrinkage of bandgap value as well as direct–indirect bandgap transformation. Organic–inorganic hybrid bismuth PVK $(CH_3NH_3)_3Bi_2Br_9$, possessing the same trigonal $P\bar{3}m1$ symmetry, was experimentally studied under high pressure, and a shrinkage of bandgap value was observed, in accordance with our result [26].

Besides $Cs_3Bi_2Br_9$, bismuth-silver DPVK $Cs_2BiAgBr_6$ is also a kind of typical and promising Bi-based PVK. Unlike $Cs_3Bi_2Br_9$, $Cs_2BiAgBr_6$ has a cubic lattice and a three-dimensional (3D) network, similar

to conventional Pb-based PVKs. Unstrained $Cs_2BiAgBr_6$ is optimized and its electronic characteristics are investigated (Fig. 4). The crystal structure of $Cs_2BiAgBr_6$ is cubic with space group $Fm\bar{3}m$, where $[BiBr_6]$ and $[AgBr_6]$ octahedra arrange orderly, with Cs cations occupying the space among the octahedra. The DOS analysis of $Cs_2BiAgBr_6$ demonstrates that Br-p orbitals and Ag-d orbitals mainly contribute to the VBM, in the meantime, Bi-p orbitals, Ag–s orbitals, and Br-p orbitals mainly contribute to the CBM. The VBM locates at point X, whereas the CBM locates at point Γ, resulting in an indirect bandgap, agreed with experimental reports, and the bandgap is calculated as 1.34 eV, lower than that of experimental reports [27]. It is commonly observed that the PBE functionals will underestimate the bandgaps of PVKs [28].

After a basic theoretical characterization, strains are applied on $Cs_2BiAgBr_6$ triaxially, and atoms are fully relaxed. In Fig. 5a–d, comparing the bandgap structures under different strains, we observe that the CBM locates at L point with tiny variation, but the VBM located at X point changes significantly under different strains. A tensile strain will enlarge the bandgap, as well as flatten the VBM, which are attributed to the more isolated octahedra than those in unstrained $Cs_2BiAgBr_6$. Similarly, a compressive strain will sharpen the energy variation in valence bands and raise VBM located at point X, subsequently shrinking the bandgap. Similar theoretical work about DPVKs shows the same tendency under high-pressure [15], and experimental work of high-pressure on $Cs_2BiAgBr_6$ exhibits a smaller bandgap value [29]. Likely, the change of bond lengths is supposed as the key factor. Therefore, the bond lengths under strain are exhibited in Fig. 5e. Due to the higher symmetry of $Cs_2BiAgBr_6$ than that of $Cs_3Bi_2Br_9$, the crystal structure is kept well under different applied strains. Except for the bond lengths, the regular octahedra are unaffected, and the Ag and Bi atoms are in the centers of regular octahedra, indicating the stability of $Cs_2BiAgBr_6$ under strains. The bond lengths of Ag–Br and Bi–Br shrink under compressive strains and enlarge under tensile strains, and it is easily observed that the bond length variation of Ag–Br is vigorous than that of Bi–Br. With a combination of DOS mentioned above, where a hybrid of Ag-d and Br-p orbitals is dominant in VBM, we indicate the sharp bond length variation of Ag–Br may mainly lead a distinct change of VBM.

According to the calculated results demonstrated above, as depicted in Fig. 5f, the applied strains effectively modify the bandgaps of both $Cs_3Bi_2Br_9$ and $Cs_2BiAgBr_6$. Strains applied on PVKs will lead the shifts of atoms and exhibit influences on bandgap, but for different PVKs, distinct results are easily observed. For example, applying biaxial strains on conventional lead PVK $CH_3NH_3PbI_3$ in DFT calculations, the largest bandgap value appears without strain, and the bandgap value decreases under both tensile and compressive strains, which is attributed to the shift of $CH_3NH_3^+$ cations approaching iodine atoms [10]. For lead-free PVK $Cs_2AgInCl_6$, the bandgap value increases monotonically from compressive to tensile strains, which is in line with our results [14]. In the meantime, the DOS corresponding to a certain band is also of great importance in optical absorption. A higher DOS will provide sufficient available states, and photons with certain energy will be adequately utilized. Therefore, DOS variations also need a detailed study. From Fig. 6a, b, we observe that under strain from tensile to compressive,

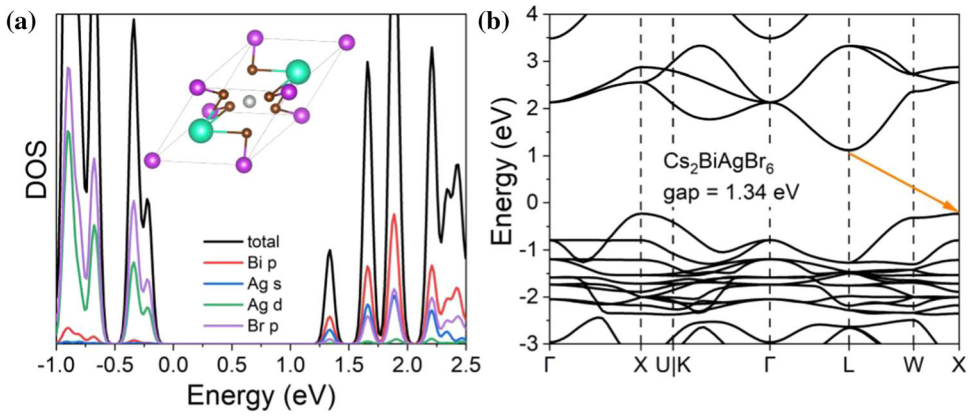

Figure 4 **a** The diagram of DOS of unstrained $Cs_2BiAgBr_6$. Inset: the diagram of the unstrained $Cs_2BiAgBr_6$ structure. **b** The diagram of the band structure of unstrained $Cs_2BiAgBr_6$.

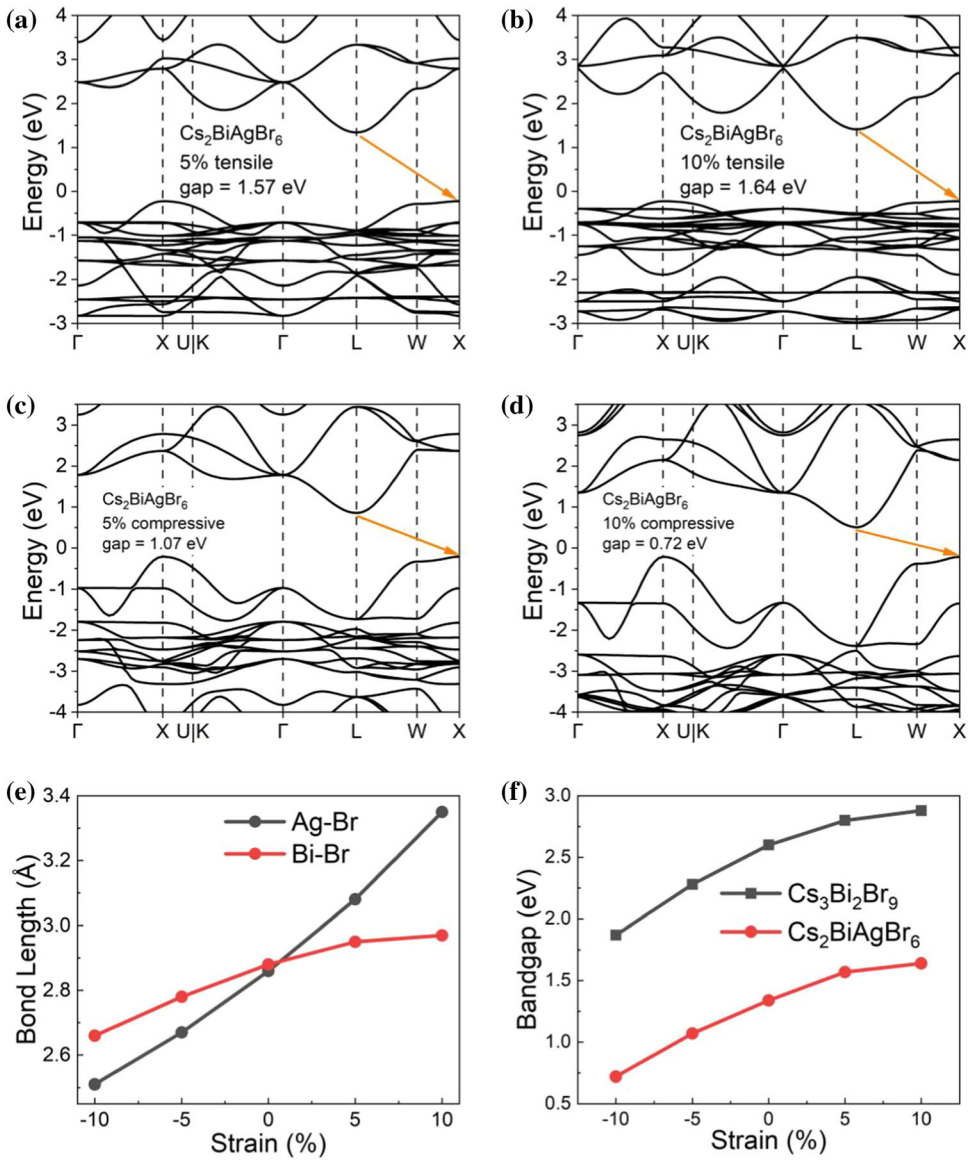

Figure 5 The band structures of $Cs_2BiAgBr_6$: under **a** 5% tensile, **b** 10% tensile, **c** 5% compressive and **d** 10% compressive strains, respectively. **e** Ag–Br and Bi–Br bond lengths in $Cs_2BiAgBr_6$ under strains. **f** Theoretical bandgap variations of $Cs_3Bi_2Br_9$ and $Cs_2BiAgBr_6$ under strains.

the main peaks of DOS of valence bands move away from the Fermi level, in both $Cs_3Bi_2Br_9$ and $Cs_2BiAgBr_6$. In the meantime, multiple tiny state peaks appear near the Fermi level in $Cs_2BiAgBr_6$ under compressive strains, corresponding to the lower bandgap, whereas these tiny state peaks will not contribute much in the light absorption.

To evaluate the light absorption abilities of $Cs_3Bi_2Br_9$ and $Cs_2BiAgBr_6$ under different strains straightway, the absorption spectra are determined followed. The complex relative dielectric constant can be expressed as $\tilde{\varepsilon} = \varepsilon_1 + i\varepsilon_2$, where ε_1 and ε_2 are the real and imaginary components of dielectric tensor, and the complex refractive index is expressed as $\tilde{n} = n + i\kappa$, where n is normal refractive index and κ is extinction coefficient. Because $\tilde{n}^2 = \tilde{\varepsilon}$ derived from Maxwell's equations, the dielectric tensors are represented as $\varepsilon_1 = n^2 - \kappa^2$ and $\varepsilon_2 = 2n\kappa$, deriving $\kappa = \frac{1}{\sqrt{2}}\left(\sqrt{\varepsilon_1^2(\omega) + \varepsilon_2^2(\omega)} - \varepsilon_1(\omega)\right)^{\frac{1}{2}}$. According to Beer's law, the absorption coefficient is concluded as $\alpha(\omega) = \frac{2\kappa\omega}{c} = \frac{\sqrt{2}\omega}{c}\left(\sqrt{\varepsilon_1^2(\omega) + \varepsilon_2^2(\omega)} - \varepsilon_1(\omega)\right)^{\frac{1}{2}}$, which will be appropriate for our simulations of absorption spectra [30, 31]. The absorption spectra are exhibited in Fig. 6c, d. In regard to $Cs_3Bi_2Br_9$, the absorption spectra match well with both energy bands and DOS; $Cs_3Bi_2Br_9$ under 10% compressive strain shows the narrowest bandgap, corresponding to an absorption below 2.0 eV. With the variation from compression to

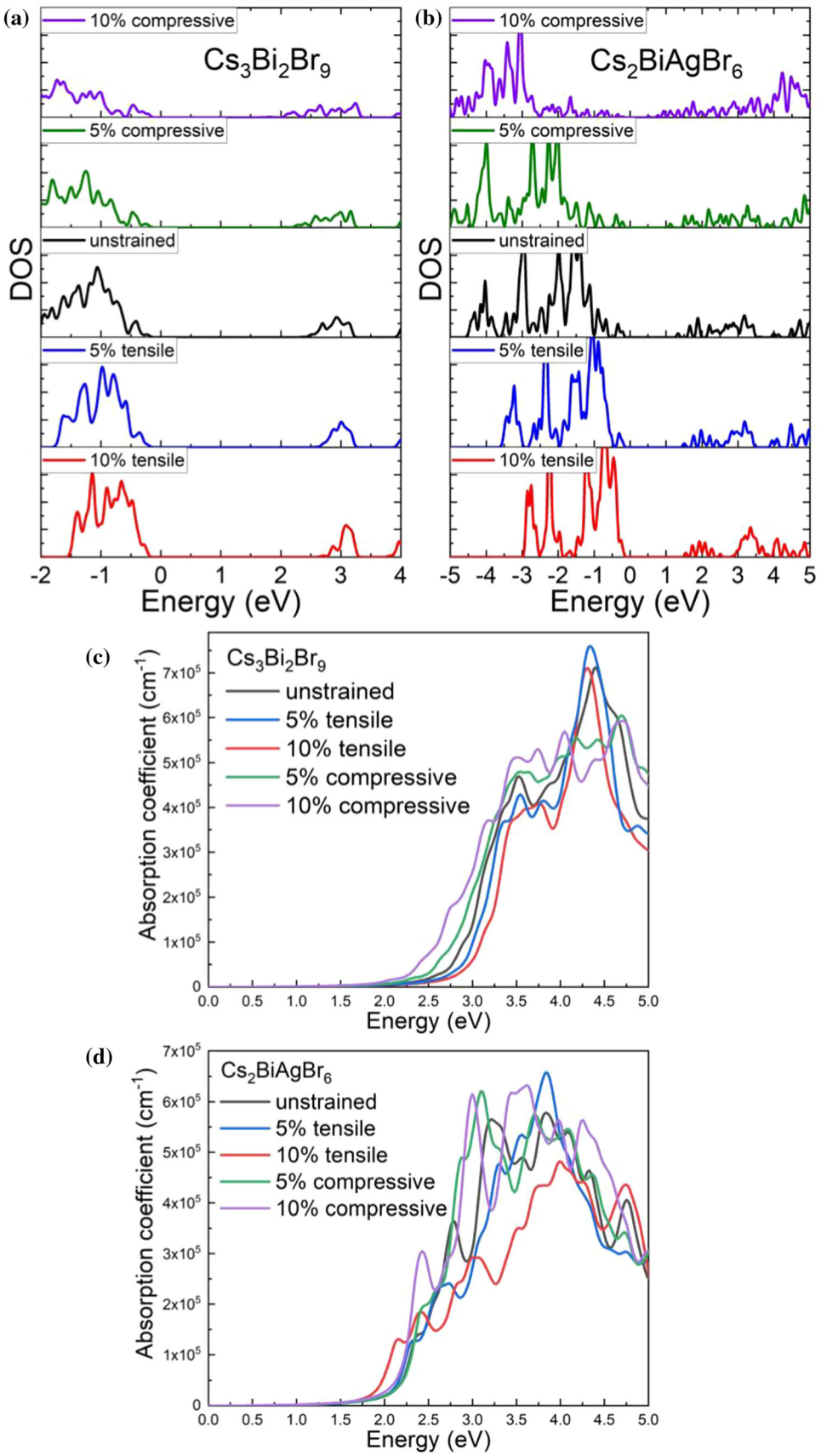

Figure 6 The DOS as well as absorption spectra of **a**, **c** $Cs_3Bi_2Br_9$ and **b**, **d** $Cs_2BiAgBr_6$ under different strains, respectively.

tension, the absorption edges gradually move to a higher energy region. However, for $Cs_2BiAgBr_6$ under compressive strain, the energy bands near VBM contribute little in photon absorptions. It is because these bands correspond to smaller DOS values compared with main peaks. As a result, the calculated absorption spectra do not match the bandgap variation tendency well, i.e., $Cs_2BiAgBr_6$ under 10% tensile strain has an obvious absorption edge in lower energy region than that under other situations.

Conclusion

In conclusion, we have investigated the influence of strains on $Cs_3Bi_2Br_9$ and $Cs_2BiAgBr_6$, where strains distinctly impact their structural, electronic and optical properties. The bandgaps of both $Cs_3Bi_2Br_9$ and $Cs_2BiAgBr_6$ shrink under compressive strains and enlarge under tensile strains. For $Cs_3Bi_2Br_9$, the band edge transition varies from direct to indirect under compressive strains and remains a direct one under tensile strains. For $Cs_2BiAgBr_6$, the band edge transition remains indirect and the positions of VBM and CBM are retained. The absorptions of $Cs_3Bi_2Br_9$ and $Cs_2BiAgBr_6$ are also investigated; $Cs_3Bi_2Br_9$ shows an accordant variation of absorption edges with bandgaps. However, the absorption edges and bandgaps of $Cs_2BiAgBr_6$ under different strains exhibit discrepancies, indicating DOS plays a key role in the absorption. Our work elaborates on the influences of strains on two kinds of promising Bi-based PVKs, and offers guidance about the strain engineering, e.g., broadening the absorption regions, in Bi-based PVKs applications for improved device performances.

Acknowledgements

This work is supported by the National Natural Science Foundation of China (Nos. U1737109, 11933006) and the Key Research and Development Program of Zhejiang Province, China (No. 2020C01120).

Declarations

Conflict of interest The authors declare no conflicts of interest.

References

[1] Liu Y, Yang Z, Liu SF (2018) Recent Progress in single-crystalline perovskite research including crystal preparation, property evaluation, and applications. Adv Sci (Weinh) 5(1):1700471. https://doi.org/10.1002/advs.201700471

[2] Xiao Z, Song Z, Yan Y (2019) From lead halide perovskites to lead-free metal halide perovskites and perovskite derivatives. Adv Mater 31(47):1803792. https://doi.org/10.1002/adma.201803792

[3] Chatterjee S, Pal AJ (2018) Influence of metal substitution on hybrid halide perovskites: towards lead-free perovskite solar cells. J Mater Chem A 6:3793–3823. https://doi.org/10.1039/c7ta09943f

[4] Attique S, Ali N, Ali S et al (2020) A potential checkmate to lead: bismuth in organometal halide perovskites, structure, properties, and applications. Adv Sci (Weinh) 7(13):1903143. https://doi.org/10.1002/advs.201903143

[5] Zhao X-G, Yang D, Ren J-C, Sun Y, Xiao Z, Zhang L (2018) Rational design of halide double perovskites for optoelectronic applications. Joule 2:1662–1673. https://doi.org/10.1016/j.joule.2018.06.017

[6] Guo L, Xu G, Tang G, Fang D, Hong J (2020) Structural stability and optoelectronic properties of tetragonal MAPbI3 under strain. Nanotechnology 31(22):225204. https://doi.org/10.1088/1361-6528/ab7679

[7] Martin LW, Chu YH, Ramesh R (2010) Advances in the growth and characterization of magnetic, ferroelectric, and multiferroic oxide thin films. Mater Sci Eng R Rep 68:89–133. https://doi.org/10.1016/j.mser.2010.03.001

[8] Amorim B, Cortijo A, de Juan F et al (2016) Novel effects of strains in graphene and other two dimensional materials. Phys Rep 617:1–54. https://doi.org/10.1016/j.physrep.2015.12.006

[9] Chen Y, Lei Y, Li Y et al (2020) Strain engineering and epitaxial stabilization of halide perovskites. Nature 577:209–215. https://doi.org/10.1038/s41586-019-1868-x

[10] Al-Shami A, Lakhal M, Hamedoun M et al (2018) Tuning the optical and electrical properties of orthorhombic hybrid perovskite CH3NH3PbI3 by first-principles simulations: strain-engineering. Sol Energy Mater Sol Cells 180:266–270. https://doi.org/10.1016/j.solmat.2017.06.047

[11] Wang S, Gong Z, Li G et al (2020) The strain effects in 2D hybrid organic-inorganic perovskite microplates: bandgap, anisotropy and stability. Nanoscale 12:6644–6650. https://doi.org/10.1039/d0nr00657b

[12] Tu Q, Spanopoulos I, Hao S et al (2019) Probing Strain-induced band gap modulation in 2D hybrid organic-inorganic perovskites. ACS Energy Lett 4:796–802. https://doi.org/10.1021/acsenergylett.9b00120

[13] Xia M, Yuan J-H, Luo J et al (2020) Two-dimensional perovskites as sensitive strain sensors. J Mater Chem C 8:3814–3820. https://doi.org/10.1039/c9tc06437k

[14] Soni A, Bhamu KC, Sahariya J (2020) Investigating effect of strain on electronic and optical properties of lead free double perovskite Cs2AgInCl6 solar cell compound: a first principle calculation. J Alloy Compd. https://doi.org/10.1016/j.jallcom.2019.152758

[15] Yang E, Luo X (2020) Theoretical pressure-tuning bandgaps of double perovskites A2(BB') X6 for photo-voltaics. Sol Energy 207:165–172. https://doi.org/10.1016/j.solener.2020.05.104

[16] Perdew JP, Burke K, Ernzerhof M (1996) Generalized gradient approximation made simple. Phys Rev Lett 77(18):3865–3868. https://doi.org/10.1103/PhysRevLett.77.3865

[17] Blöchl PE (1994) Projector augmented-wave method. Phys Rev B 50(24):17953–17979. https://doi.org/10.1103/PhysRevB.50.17953

[18] Kresse G, Furthmüller J (1996) Efficient iterative schemes for ab initio total-energy calculations using a plane-wave basis set. Phys Rev B 54(16):11169–11186. https://doi.org/10.1103/PhysRevB.54.11169

[19] Momma K, Izumi F (2011) VESTA 3 for three-dimensional visualization of crystal, volumetric and morphology data. J Appl Crystallogr 44:1272–1276. https://doi.org/10.1107/S0021889811038970

[20] Nelson RD, Santra K, Wang Y, Hadi A, Petrich JW, Panthani MG (2018) Synthesis and optical properties of ordered-vacancy perovskite cesium bismuth halide nanocrystals. Chem Commun (Camb) 54:3640–3643. https://doi.org/10.1039/c7cc07223f

[21] Lou Y, Fang M, Chen J, Zhao Y (2018) Formation of highly luminescent cesium bismuth halide perovskite quantum dots tuned by anion exchange. Chem Commun (Camb) 54:3779–3782. https://doi.org/10.1039/c8cc01110a

[22] Gao M, Zhang C, Lian L et al (2019) Controlled synthesis and photostability of blue emitting Cs3Bi2Br 9 perovskite nanocrystals by employing weak polar solvents at room temperature. J Mater Chem C 7:3688–3695. https://doi.org/10.1039/c9tc00400a

[23] Luo T, Wei J (2020) First principles study of electronic and optical properties of inorganic and lead-free perovskite: Cs3Bi2X9 (X: Cl, Br, I). Mater Chem Phys. https://doi.org/10.1016/j.matchemphys.2020.123374

[24] Luo Z, Li Q, Zhang L et al (2020) 0D Cs3 Cu2 X5 (X = I, Br, and Cl) nanocrystals: colloidal syntheses and optical properties. Small 16(3):1905226. https://doi.org/10.1002/smll.201905226

[25] Zhu D, Zaffalon ML, Pinchetti V et al (2020) Bright Blue emitting Cu-doped Cs2ZnCl4 colloidal nanocrystals. Chem Mater 32:5897–5903. https://doi.org/10.1021/acs.chemmater.0c02017

[26] Li Q, Yin L, Chen Z et al (2019) High Pressure structural and optical properties of two-dimensional hybrid halide perovskite (CH3NH3)3Bi2Br 9. Inorg Chem 58:1621–1626. https://doi.org/10.1021/acs.inorgchem.8b03190

[27] Slavney AH, Hu T, Lindenberg AM, Karunadasa HI (2016) A bismuth-halide double perovskite with long carrier recombination lifetime for photovoltaic applications. J Am Chem Soc 138:2138–2141. https://doi.org/10.1021/jacs.5b13294

[28] Jacobs R, Luo G, Morgan D (2019) Materials Discovery of stable and nontoxic halide perovskite materials for high-efficiency solar cells. Adv Func Mater. https://doi.org/10.1002/adfm.201804354

[29] Li Q, Wang Y, Pan W et al (2017) High-Pressure band-gap engineering in lead-free Cs2 AgBiBr 6 double perovskite. Angew Chem Int Ed Engl 56:15969–16189. https://doi.org/10.1002/anie.201708684

[30] Amin B, Ahmad I, Maqbool M, Goumri-Said S, Ahmad R (2011) Ab initio study of the bandgap engineering of Al1−xGaxN for optoelectronic applications. J Appl Phys 109(2):023109. https://doi.org/10.1063/1.3531996

[31] Fox M (2001) Optical Properties of Solids. Oxford University Press, New York